

Noncontact In-Bed Measurements of Physiological and Behavioral Signals Using an Integrated Fabric-Sheet Sensing Scheme

Mayuko Takano¹, Student Member, IEEE, and Akinori Ueno², Member, IEEE

Abstract—Home monitoring requires measuring the physiological and behavioral signals without impairing a subject's everyday life. This paper presents an integrated and noncontact approach for obtaining simultaneous physiological and behavioral signals of recumbent humans in beds using a home-monitoring application. In the proposed approach, a fabric-sheet unified sensing electrode (FUSE) obtains physiological signals by recording the electrocardiogram (ECG), chest and abdominal respiratory movements (RMs), and ballistocardiogram (BCG). The FUSE also detects the behavioral signals of body proximity (BPx) and lateral/supine lying postures. A prototype system with FUSE was validated in a short-term experiment and 6-h overnight measurements on two different groups composed of seven lying subjects. The results confirmed that the approach senses each signal independently and records the ECG, RMs, BCG, and BPx signals simultaneously. The mean sensitivities of the *R* and *T* waves of the ECG during sleep were 86.1% and 88.0%, respectively, whereas those of the chest and abdominal RMs were 90.7% and 90.1%, respectively. Although our prototype system has room for improvement, the results suggest that our approach enables the unconstrained, nocturnal monitoring of the physiological and behavioral signals in recumbent humans. The at-home monitoring of the physiological and behavioral signals is expected to contribute to cost-effective personalized healthcare in the future. This noncontact and easy-to-install system for in-bed measurements can facilitate a new era of home monitoring.

Index Terms—Capacitive electrocardiography (cECG), respiratory movements, ballistocardiogram (BCG), body proximity, lying posture, home monitoring, unobtrusive measurements, vitals monitoring, fall prevention, pressure ulcer prevention.

I. INTRODUCTION

ACCORDING to a 2007 United Nations demographic survey, the proportion of the world's population aged 60 and above is expected to grow by up to 21.8% between 2007 and 2050 [1]. Given the rapidly aging population [2] along with the advances in information and communication technologies and artificial intelligence, the physiological and behavioral signals will be realistically monitored at home in the near future. Such at-home monitoring would play an important role in both preventive daily healthcare and post-hospital medical care [3], [4]. The growing number of patients with chronic cardiorespiratory conditions, such as heart failure [5], atrial fibrillation [6], and sleep apnea [7], gives more urgency to this expectation. The evidence from clinical trials demonstrates that management programs, including home monitoring, improve clinical outcomes, particularly for patients hospitalized with heart failure (HF) [8]. The United States Veterans Health Administration introduced a large-scale (national), enterprise-wide home telehealth program and found that it effectively managed chronic care patients at a reasonable cost in both urban and rural settings [9].

Electrocardiograph (ECG) signals are among the most crucial physiological signals to be monitored because cardiovascular disease (CVD) is the leading cause of death in the United States [5] and coronary heart disease (CHD) is the leading cause of death worldwide [10]. Abnormalities in the baseline ECG are strongly associated with subsequent CVD and CHD mortalities of all types [11]. In addition to ECG signals, it is important to monitor the respiratory movements (RMs) because sleep-disordered breathing is associated with acute unfavorable effects on cardiovascular physiology [7]. Bennet *et al.* [12] studied the recumbent nocturnal physiological patterns of older adults discharged to their homes after hospitalization for HF. Their findings indicated that respiratory rate (RR) is the most important risk-adjusted indicator of readmission for HF [12]. The ballistocardiogram (BCG) is another important physiological signal because the interval between the R-wave peak of the ECG and the J-wave peak of the BCG (i.e., the RJ interval) is strongly correlated with the heart's pre-ejection period [13], [14], which is a useful indicator of the heart's contractility [15] and can be used to determine left ventricular performance in patients with CVD [16]. In addition, the BCG might provide the relative stroke volume of the heart [14], [17] and/or the systolic blood pressure [18].

Manuscript received December 1, 2017; revised March 6, 2018; accepted March 30, 2018. Date of publication May 7, 2018; date of current version March 6, 2019. This work was supported in part by the Strategic Research Foundation Grant-aided Project for Private Universities from Ministry of Education, Culture, Sport, Science and Technology, Japan, 2015–2017 (S1512001) and in part by SECOM Science and Technology Foundation. (Corresponding author: Mayuko Takano.)

M. Takano is with the Master's Program in Electric and Electronic Engineering, Tokyo Denki University, Tokyo 120-8551, Japan (e-mail: uenolab_takano@uenolab.jp).

A. Ueno is with the Department of Electrical and Electronic Engineering, Tokyo Denki University, Tokyo 120-8551, Japan (e-mail: ueno@mail.dendai.ac.jp).

Digital Object Identifier 10.1109/JBHI.2018.2825020

When monitoring behavioral signals, it is essential to monitor bed-entering and bed-exiting body movements because falls commonly occur around beds in both hospitals and residential care facilities [19]–[21], especially during attempts to enter or leave the bed [22], [23]. Elderly people worldwide are vulnerable to falls and fall-induced injuries [24], and the burden and cost of falls are expected to increase as populations age [25]–[27]. A signal that reflects body posture could also prevent the development of pressure ulcers in immobilized patients or frail elderly patients in home care settings. Pressure ulcers can cause a number of adverse health outcomes such as increased morbidity and mortality and reduced quality of life. Pressure ulcers also represent a significant financial burden to the National Health Service [28]–[30]. Moreover, by monitoring body posture signals, caregivers could evaluate changes in the sleeping postures of patients with obstructive sleep apnea (OSA). This is important because OSA events occur more frequently and severely in the supine posture compared to in other postures [31], [32].

During home monitoring, patients' physiological and behavioral signals must be measured without disrupting their everyday lives using ambient and unobtrusive methods. Moreover, for the monitoring equipment to be easily introduced and maintained, it will likely be necessary to integrate several measurement methods. Based on these considerations, we propose an integrated noncontact approach for in-bed measurements of physiological and behavioral signals, namely: ECG, RM, BCG, body proximity (BPx), and lying posture (LP). The approach is based on a newly devised fabric-sheet unified sensing electrode (FUSE). The viability of the proposed approach is tested using a prototype measurement device and pilot FUSE in both brief and prolonged laboratory experiments.

II. RELATED WORKS

Many noncontact in-bed measurement methodologies have been proposed for monitoring physiological and/or behavioral signals [33]. Capacitive electrodes [34], [35] are promising devices for biopotential measurements, particularly ECG measurements [36], [37]. Capacitive electrodes made of conductive fabric and placed under a bed sheet can also measure RMs [38], [39]. Capacitive electrodes can also be used to measure ECG (cECG) simultaneously with LP or BPx [40], [41]. Thus, cECG and a second physiological or behavioral signal were successfully detected in the above studies; however, the simultaneous detection of three or more signals has not yet been reported.

When the target application allows the ECG to be substituted by another cardiomechanical signal (e.g., BCG or seismocardiogram), piezoelectric or acceleration sensors are usually used [42]. These sensors can measure multiple signals in the absence of ECG signals [43]–[46], and some proposed sensor systems are in the clinical validation phase. Therefore, if a piezoelectric or acceleration sensor could be developed from the same conductive fabrics as used in conventional capacitive electrodes and combined with a capacitive electrode, we could realize a large-scale, high-integrity tool for measuring physiological and behavioral signals.

III. MATERIALS AND SYSTEMS

A. Fabric-Sheet Unified Sensing Electrode (FUSE)

The FUSE was designed for simultaneous measurements of cECG, BPx, RM, and BCG signals. The FUSE is placed under the bed sheet, beneath the back of the lying subject. To prevent sleep disruption, the FUSE is constructed from thin, soft materials (conductive fabric and insulating textiles; see Fig. 1). The laminated structure [Fig. 1(a)] suppresses common-mode noise and electromagnetic disturbance [47], [48] in the cECG measurements and mitigates the interference between the cECG and other measured signals. The inner electrodes (1) and (2) in Fig. 1 were introduced only for cECG measurements and are arranged in parallel up and down the subject's heart. The driven shields (6) and (7) surrounding each inner electrode are connected to the output terminals of separate bootstrapped voltage followers. The signal ground layer (5) provides double shielding to both sets of the inner electrode and a driven shield. Layer (5) functions as a capacitive ground (cGND) when coupled with the conductive trunk or upper body of the lying subject. It also plays the role of two capacitive sensors in combination with the outer electrodes (3) and (4). The outer electrodes are placed at the shoulder and lower back of the subject for independent BPx and RM measurements of the chest and abdomen. The capacitive sensor, including the outer electrode (3), is intended for BCG measurements. To prevent electrode displacement and overlap during repeated body movements such as rolling, the electrodes and shielding structures are unified into a unit on a base sheet constructed of insulating textile.

B. cECG Measurement

In our proposed layout, the inner electrodes coupled to the upper body through the subject's clothing are considered as two capacitive couplings with capacitances C_1 and C_2 , as shown in Fig. 2(a). According to the corresponding connection in Fig. 1(b), the cECG is passively measured as the difference between the potentials at coupling points 1 and 2 ($v_{\text{cECG}(1)}$ and $v_{\text{cECG}(2)}$, respectively). To suppress the voltage drops from $v_{\text{ECG}(1)}$ to $v_{\text{cECG}(1)}$ and from $v_{\text{ECG}(2)}$ to $v_{\text{cECG}(2)}$, voltage followers with high input impedance are typically placed at the front ends of the following detection circuit [37], [49]. Here, we installed bootstrapped voltage followers at the front ends; these voltage followers maintain high input impedance only to AC signals and shorten the baseline restoration time after body movements such as rolling [39]. The frequency band of the cECG was set at 0.5–100 Hz, and the amplifier gain was set to 60 dB.

C. Measurements of BPx, LP, RM, and BCG

The outer electrodes and signal ground layer, which are coupled to the upper body through the subject's clothing, can be deemed as three capacitive couplings with capacitances $C_{\text{BPx}(3)}$, $C_{\text{BPx}(4)}$, and C_G , as shown in Fig. 2(b). In the upper panel of Fig. 1(b), series-connected capacitors $C_{\text{BPx}(3)}$ and C_G are incorporated in an astable multivibrator commonly used in $\text{BPx}_{\text{chest}}$, RM_{chest} , and $\text{BCG}_{\text{chest}}$ detection. The

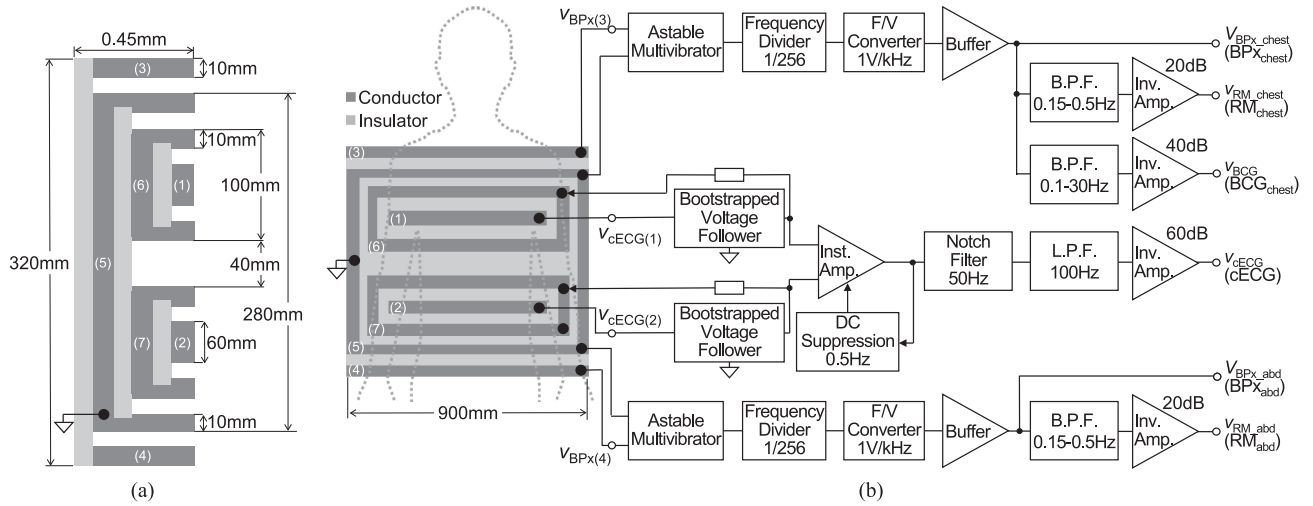


Fig. 1. The proposed measuring system. (a) Cross-sectional configuration of the FUSE. The top layers (1) and (2) are the electrodes for cECG measurement, and layers (6) and (7) are driven shields that receive the output of the bootstrapped voltage followers as feedback. The electrodes are doubly shielded by the third and fifth layers of the circuit ground (5), which also detect the BCG. Additional outer electrodes (3) and (4) detect the BPx and RM signals combined with the circuit ground (5). (b) Top-view configuration of the FUSE and block diagram of the proposed measuring system. The FUSE is placed under the bed sheet with the upper outer electrode (3) positioned beneath the upper edges of both shoulders. The cECG detection system comprises two bootstrapped voltage followers, an instrumentation amplifier with DC suppression, filters, and amplifiers. The BPx detection circuit consists of an astable multivibrator, a frequency divider, an F/V converter, and a buffer. The RM and BCG signals are derived from a common BPx signal through corresponding bandpass filters.

multivibrator oscillates at a specific frequency depending on the net capacitance $C_{net(3)}$ of the series-connected capacitor. When $C_{BPx(3)} \ll C_G$ in the FUSE, $C_{net(3)}$ can be approximated by $C_{BPx(3)}$, as shown in (1):

$$C_{net(3)} = \frac{C_{BPx(3)} C_G}{C_{BPx(3)} + C_G} = \frac{C_{BPx(3)}}{1 + \frac{C_{BPx(3)}}{C_G}} \approx C_{BPx(3)}. \quad (1)$$

The oscillatory frequency $f_{osc(3)}$ of the multivibrator depends on $C_{BPx(3)}$:

$$f_{osc(3)} = \frac{k_{osc}}{R_3 C_{net(3)}} \approx \frac{k_{osc}}{R_3 C_{BPx(3)}}, \quad (2)$$

where R_3 is the resistance (Ω) in Fig. 2(b), and k_{osc} is a constant determined by the power-supply voltage and threshold voltages of the Schmitt inverter integrated circuit (National Semiconductor, LM231) in Fig. 2(b). The output voltage $V_{out(3)}$ of the frequency-to-voltage (F/V) converter is proportional to the input frequency $f_{osc(3)}$ as follows:

$$V_{out(3)} = k_{fv} \cdot f_{osc(3)} \approx \frac{k_{fv} k_{osc}}{R_3 C_{BPx(3)}}, \quad (3)$$

where the proportionality factor k_{fv} is determined by the resistance and capacitance in the F/V converter circuit. To calculate $C_{BPx(3)}$, we need the permittivity of the coupling ε [F·m], the coupling area $A_{S(3)}$ [m²], and the coupling distance $d_{S(3)}$ [m]. The coupling distance is the sum of three time-varying distances $d_{(3)BPx}$, $\Delta d_{(3)RM}$, and $\Delta d_{(3)BCG}$. Specifically, $C_{BPx(3)}$ is calculated as

$$C_{BPx(3)} = \varepsilon \frac{A_{S(3)}}{d_{S(3)}} = \varepsilon \frac{A_{S(3)}}{d_{(3)BPx} + \Delta d_{(3)RM} + \Delta d_{(3)BCG}}, \quad (4)$$

where $d_{(3)BPx}$ is the distance between the upper body and outer electrode (3) determined by the lying or rising posture. The distance changes $\Delta d_{(3)RM}$ and $\Delta d_{(3)BCG}$ are caused by respiration-associated chest movements and ballistocardiographic displacement, respectively. Substituting (4) into (3), we obtain

$$V_{out(3)} \approx \frac{k_{fv} k_{osc}}{R_3 \varepsilon} \cdot \frac{d_{(3)BPx} + \Delta d_{(3)RM} + \Delta d_{(3)BCG}}{A_{S(3)}}. \quad (5)$$

When a subject's upper body moves up or down (e.g., when entering or exiting the bed), the change in $d_{(3)BPx}$ dominates $\Delta d_{(3)RM}$ and $\Delta d_{(3)BCG}$. Under this condition, the output voltage $V_{out(3)}$ is calculated as

$$V_{out(3)} \approx \frac{k_{fv} k_{osc}}{R_3 \varepsilon} \cdot \frac{d_{(3)BPx}}{A_{S(3)}} \equiv V_{BPx_chest}. \quad (6)$$

Note that (6) includes the coupling term $A_{S(3)}$. When the subject changes his/her body position to or from the lateral posture, the change in $1/A_{S(3)}$ dominates $d_{(3)BPx}$. Therefore, V_{BPx_chest} reflects not only BPx, but also LP around the chest.

When the subject maintains a steady body posture, both $d_{(3)BPx}$ and $A_{S(3)}$ can be regarded as constants. The change in output voltage $\Delta V_{out(3)}$ is then sensitive to $\Delta d_{(3)RM}$ and $\Delta d_{(3)BCG}$ and can be expressed as follows:

$$\Delta V_{out(3)} \propto \frac{k_{fv} k_{osc}}{R_3 \varepsilon A_{S(3)}} (\Delta d_{(3)RM} + \Delta d_{(3)BCG}) \equiv v_{RM_chest} + v_{BCG_chest}, \quad (7)$$

where v_{RM_chest} and v_{BCG_chest} are the components of $\Delta V_{out(3)}$ sensitive to RM and BCG, respectively, at the chest. As v_{RM_chest}

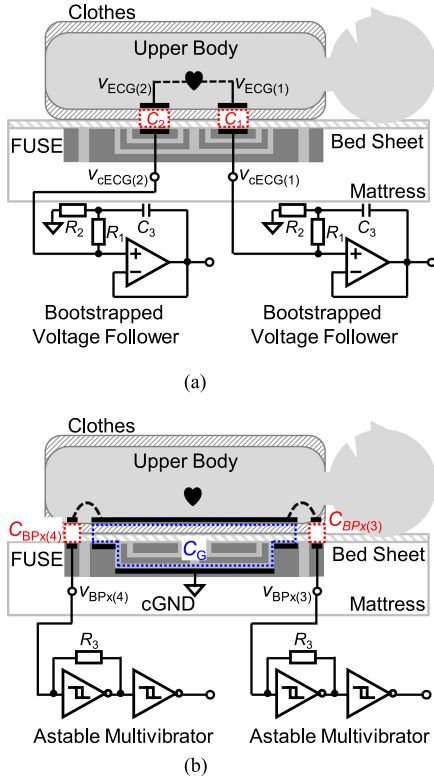


Fig. 2. Schematic of the capacitive couplings associated with the measurement principle of the proposed approach. The couplings consist of the volume conductor of the lying subject, insulating materials (bed sheet and clothes worn by the subject), and the conductive fabric in the FUSE. (a) Couplings related to cECG measurement. The heart represents a voltage source in the volume conductor, which generates voltages $v_{ECG(1)}$ and $v_{ECG(2)}$ via the couplings. The cECG is the potential difference between $v_{cECG(1)}$ and $v_{cECG(2)}$. (b) Couplings involved in the BPx, RM, and BCG measurements. The series connections of $C_{BPx(3)}$ and C_G , and $C_{BPx(4)}$ and C_G are incorporated in the astable multivibrator circuits, resulting in square pulses $v_{BPx(3)}$ and $v_{BPx(4)}$, respectively. The frequencies of $v_{BPx(3)}$ and $v_{BPx(4)}$ depend on the combined capacitances of $C_{BPx(3)}$ and C_G , and $C_{BPx(4)}$ and C_G , respectively.

and v_{BCG_chest} have different frequency components, they can be derived from their corresponding frequency filters [see the block diagram in Fig. 1(b)]. The frequency bands of v_{RM_chest} and v_{BCG_chest} were set to 0.15–0.5 and 0.1–40 Hz, respectively.

By considering the series-connected capacitors $C_{BPx(4)}$ and C_G , we can similarly determine V_{BPx_abd} , v_{RM_abd} , and v_{BCG_abd} , which are sensitive to BPx and RM, respectively, at the abdomen (BPx_{abd} and RM_{abd}).

IV. EXPERIMENTAL AND ANALYTICAL METHODS

All experimental procedures were approved by the Human Life Ethics Committee of Tokyo Denki University. All subjects provided informed consent prior to participation in our experiments. The subjects were accepted onto the study if they had no prior medical history of cardiopulmonary or cardiovascular disease. The measuring system is shown in Fig. 1(b). All signals obtained by the system were digitized at 1 kHz with 16-bit resolution, with a view to future precise analysis. The reference voltage was ± 10 V. All subjects wore commercially available nightwear made from 0.36-mm-thick cotton and slept on

commercially available cotton bed sheets with a thickness of 0.33 mm.

A. BPx Signals With Postural Changes and Their Classification

As a fundamental evaluation of the proposed system, we measured the BPx signals at the chests (BPx_{chest}) and abdomens (BPx_{abd}) of seven subjects #A–#G [22–45 years old, 1.67–1.76 m height, 50.0–83.0 kg weight, 18.0–23.3 kg/m² in body-mass index (BMI)]. The subjects were requested to change their LP sequentially on cue and to maintain each posture for 20 s. The postural sequence was sitting, supine, left lateral, supine, right lateral, supine, and sitting. The BPx signals recorded at each posture were divided into five segments, each with a duration of 4 s. The voltages of the BPx signals at the chest (V_{BPx_chest}) and abdomen (V_{BPx_abd}) were averaged over each of the second, third, and fourth segments. Each chest–abdomen pair of mean voltages was considered as a two-dimensional datum and classified into one of three posture clusters (sitting, supine, or lateral) using a K-means clustering algorithm. The classification was performed for each subject and for all subjects together. The sensitivity (P_{SNS}), accuracy (P_{ACC}) and positive predictive value (P_{PPV}) of each cluster were calculated by (8), (9) and (10), respectively:

$$P_{SNS} = \frac{N_{TP}}{N_{TP} + N_{FN}} \times 100, \quad (8)$$

$$P_{ACC} = \frac{N_{TP} + N_{TN}}{N_{TP} + N_{TN} + N_{FP} + N_{FN}} \times 100, \quad (9)$$

and

$$P_{PPV} = \frac{N_{TP}}{N_{TP} + N_{FP}} \times 100, \quad (10)$$

where N_{TP} , N_{TN} , N_{FP} , and N_{FN} are the numbers of data correctly classified into the target cluster, correctly classified into other clusters, incorrectly classified into the target cluster, and falsely classified into other clusters, respectively.

B. Evaluation of RM Signals

We tested whether our system could measure RMs with different RRs in a single 24-year-old subject #H (1.71 m height, 61 kg weight, 20.9 kg/m² BMI) with three different LPs: supine, right lateral, and left lateral. Reference RM signals at the chest (RM_{ref_chest}) and abdomen (RM_{ref_abd}) were simultaneously measured by telemetric belt-type transducers (TSD201, BIOPAC Systems) and amplifiers (RESP100C, BIOPAC Systems). The transducers were worn on the subject's chest and abdomen. This test involved only the detection of BPx and RM [Fig. 1(b)] because the transducer worn on the chest could lead to interference in the cECG measurement. First, the subject was asked to lie on the bed in a supine position. To verify the RR, the timing of breaths was synchronized with a metronome. The measurement lasted for 90 s at each of eight fixed RRs ranging from 10 to 30 respirations per minute. With the subject lying on the bed in the right- and left-lateral postures, the RM signals were tested in the same manner.

The RM signals including reference signals were preprocessed by filtering twice through a digital bandpass filter (infinite impulse response filter, $f_c = 0.15\text{--}0.5$ Hz). Discrete RM cycles in the RM signals were automatically detected by software with threshold processing [50]. The RR was calculated for each measurement by dividing the total duration of RMs in a 10.5-cycle recording by the detected number of RMs in the recording. We then calculated the correlation coefficients for the RRs determined using our new system and those determined by the commercial system used for the reference signal measurement for the chest and abdomen in three LPs.

C. Multichannel Simultaneous Measurements in Each Body Posture

A short test in which the cECG, $BP_{x_{\text{chest}}}$, $BP_{x_{\text{abd}}}$ (i.e., RM_{chest} and RM_{abd}), and BCG signals were measured was performed on one 24-year-old subject #I (1.73 m height, 83 kg weight, 23.3 kg/m² BMI). First, the subject was asked to lie supine on the bed. Second, the subject was assigned the following sequence of postures: left lateral, supine, right lateral, and supine. All postures were held for 50 s except for the last supine posture, which was held for approximately 60 s. Finally, the subject was asked to arise and sit on the bed. The body movements of the participants were verified by video recordings.

D. Overnight Measurements

Next, our proposed system was validated through experimental measurements of seven healthy male subjects #J–#P (20–23 years old, 1.60–1.87 m height, 55.0–78.8 kg weight, 20.9–26.6 kg/m² BMI) during sleep. Reference Lead III ECG signals were measured by a commercially available ECG telemetry system (i.e., BN-RSPEC, BIOPAC Systems) and disposable electrodes (i.e., F-150S, Nihon Kohden). The reference RM signal at the abdomen ($RM_{\text{ref,abd}}$) was measured with the same telemetry system and a belt-type transducer (BN-RESP-XDCR, BIOPAC systems). In this experiment, the respiration transducer was worn only on the abdomen to avoid interference with the cECG measurement. Again, the body movements were verified by video recordings. Blood oxygen saturation (SpO_2) was measured using a commercially available transducer (TSD123A, BIOPAC Systems) and a calculation module (OXY100C, BIOPAC Systems). For advanced analysis, a sheet-type sensor of a commercial screening device of sleep apnea syndrome (Sleep EYE GD700, GAC Co., Ltd., approved in Japan) was placed under the FUSE. A software supplied with the device can detect apnea/hypopnea episode and calculate apnea–hypopnea index (AHI). At the start of the measurements, volumetric humidity was set to 6–10 g/m³. The duration of the experiment was at least 6 h, although only the data collected during the first 6 h were analyzed. The subjects were free to change body positions as they wished. The RM signals were preprocessed as described in Section IV-B. To allow comparison with the conventional system, the above-described subjects, test protocol, and preprocessing method of RM signals were set to be the same as described in a previous study [39].

Also to allow comparison with the conventional system [39], the Q wave, R wave, and peak and end of the T wave (T_{top}

and T_{end} , respectively) for the reference ECG and cECG were detected by beat-by-beat pattern matching using the wavelet transform [51]. The R–R interval (RRI) was calculated from the two consecutive detected R waves. If the RRI of a cECG signal was within ± 3 ms of the RRI of the reference ECG, the latter R wave of the cECG was deemed correctly detected. For the reference ECG, the Q–T interval (QTI) was calculated from the detected Q wave and T_{end} . Bazett compensation was performed on the QTIs obtained from the reference and our proposed system as the QTI is known to depend on RRI [52]. Subsequently, the mean (MN) and standard deviation (SD) of QTI was computed for the 6 h of analyzed data. For cECG, QTI was calculated from the Q wave of the reference ECG and detected T_{end} of the cECG. If the QTI of the cECG signal was within $MN \pm 1.96SD$ of the reference ECG, the T wave of the cECG was deemed correctly detected. The RM cycles were detected using the same software as described in Section IV-B. If the starting time of a detected RM cycle in our system was in between that of the reference signal, the RM cycle of our system was deemed correctly detected. The P_{SNS} , P_{ACC} and P_{PPV} of the ECG and RM signals were then calculated.

We investigated correlations of ECG parameters (RRI and compensated QTI) and RRs (of RM_{chest} and RM_{abd}) between the reference and our new systems during 4th 1-h segment in the 6-h recording for all subject by using a Bland–Altman plot. For this analysis, correctly detected data (N_{TP}) were only used. RRs were calculated by using reciprocal of the total duration of RMs in a 10-cycle window and by shifting the window in a breath-by-breath manner.

We tested whether any decrease in RRI associated with sleep apnea or/and hypopnea could be detected in the cECG signals. Here, we referenced an autocorrelated wave-detection algorithm with adaptive threshold provided by Hayano *et al.* [53]–[55]. First, the recorded cECG signal was differentiated. The RRI time series $X(t)$ were generated by interpolation with a spline function and resampling at 2 Hz [53]. Next, the RRI time series satisfying (11) were detected as candidate dips:

$$X(t) + \frac{\Delta t^2}{49} \leq X(t + \Delta t), \quad (-5 \leq \Delta t \leq 5). \quad (11)$$

After calculating the depths and widths of all the candidate dips, we selected those with depth-to-width ratios exceeding 0.7 ms/s [54]. In addition, the upper and lower envelopes of the RRI variations were calculated as the 95th and 5th percentile points, respectively, within a shifting window with a width of 130 s [54]. Finally, we selected the dips with depths greater than 40% of the envelope range. The same analysis was performed on the reference ECG for comparison.

V. RESULTS

A. Classification of Body Posture

Table I tabulates the classification P_{SNS} , P_{ACC} and P_{PPV} for each subject and for all subjects. The sitting postures and LPs were clearly classified in all subjects, and the supine and lateral postures were perfectly classified in four subjects. The classification results of all subjects are shown in Fig. 3. The central points in clusters 1, 2, and 3 describe the supine po-

TABLE I
SENSITIVITY (P_{SNS}) [%], ACCURACY (P_{ACC}) [%] AND POSITIVE PREDICTIVE VALUE (P_{PPV}) [%] FOR EACH BODY POSTURE

Subject	Sitting			Supine			Lateral		
	P_{SNS}	P_{ACC}	P_{PPV}	P_{SNS}	P_{ACC}	P_{PPV}	P_{SNS}	P_{ACC}	P_{PPV}
#A	100	100	100	100	100	100	100	100	100
#B	100	100	100	100	100	100	100	100	100
#C	100	100	100	100	100	100	100	100	100
#D	100	100	100	66.7	75.0	66.7	50.0	87.5	100
#E	100	100	100	100	100	100	100	100	100
#F	100	100	100	66.7	75.0	66.7	50.0	75.0	50.0
#G	100	100	100	88.9	81.8	72.7	50.0	83.3	75.0
MN±SD	100±0.0	100±0.0	100±0.0	88.9±15.7	90.2±12.4	86.6±16.9	78.6±26.7	92.3±10.3	89.3±19.7
All (A-G)	100	100	100	90.5	88.2	82.6	71.4	88.6	83.3

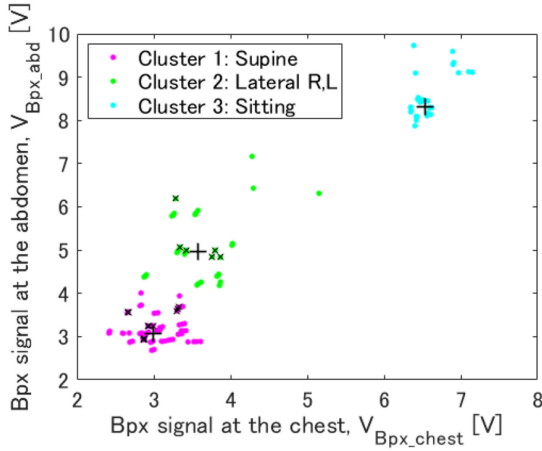


Fig. 3. Cluster plots of V_{BPx_chest} vs. V_{BPx_abd} obtained from seven subjects #A-G. Clusters 1, 2, and 3 correspond to the supine position, right- or left-lateral position, and sitting position, respectively. Crosses mark the center of gravity of each cluster. Plots with overtyped letters x indicate incorrectly clustered plots.

sition ($V_{BPx_chest} = 3.0$ V and $V_{BPx_abd} = 3.0$ V), lateral position ($V_{BPx_chest} = 3.5$ V and $V_{BPx_abd} = 5.0$ V), and sitting position ($V_{BPx_chest} = 6.6$ V and $V_{BPx_abd} = 8.4$ V), respectively. The classification P_{ACC} were 88.2% for supine posture, 88.6% for lateral posture, and 100% for sitting posture. These results indicate that FUSE can provide BPx signals that clearly indicate the presence of the trunk of the subject (i.e., volume conductor). However, further improvement is needed to distinguish between supine and lateral postures (e.g., by combining the RM and cECG signals).

B. RM Measurements on the Chest and Abdomen in Each LP

Fig. 4 shows the correlation between RRs recorded by a respiratory transducer and those measured using the proposed system on the chest and abdomen in the supine, right-lateral, and left-lateral postures. The correlation coefficient for the above three LPs on the chest were 0.97, 0.97, and 0.99, respectively, whereas those on the abdomen were 0.99, 0.93, and 0.98, respectively. In addition, root mean square errors (RMSEs) on the chest and abdomen were 1.60 and 1.99 rpm, respectively. These results confirm that our system adequately detected RMs on the chest

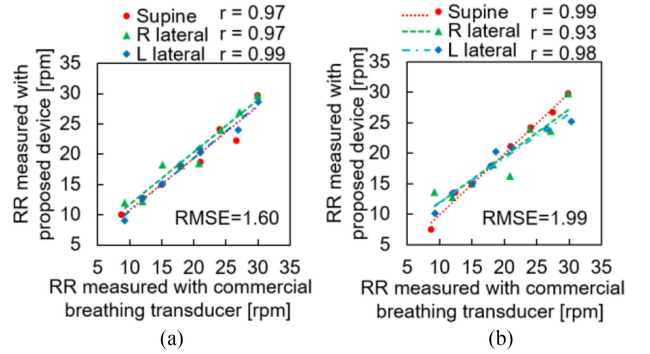


Fig. 4. Correlation between the respiratory rates (RRs) of subject #H measured by a commercial belt-type transducer and the proposed device. RRs were calculated from both the (a) chest and (b) abdominal respiratory movements (RMs). The RM intervals were regulated by and varied using a metronome.

and abdomen in three different LPs, even without band-type transducers worn on the body.

C. Simultaneous Multichannel Measurement in Each LP

Fig. 5(a) shows the continuous waveforms of the BPx, cECG, and RM signals in each body posture during the sequence of postural changes. The results confirm that our system measured all the above signals in all tested postures. The changes in LP produced noticeable changes in BPx voltage, cECG wave profile, and RM amplitude. Although periods of saturation immediately following rolling-over motions were observed in the cECG and RM signals, the baseline signals were restored in 5 and 15 s, respectively. Regarding the cECG signal quality, a commercially available software (AcqKnowledge4.1, BIOPAC Systems) automatically recognized the P, QRS, and T waves in all LPs, as shown in Fig. 5(b). The RM shape was less distorted on the abdomen than on the chest, and the phases of RM_{chest} and RM_{abd} were in the reverse in both the supine and right-lateral postures, as shown in Fig. 5(c).

D. Overnight Measurements

Fig. 6 shows example recordings of cECG and RM signals from the proposed and reference systems in each LP obtained during overnight experiment for subject #J. The cECG and RM signals were synchronized with the simultaneously measured reference signals, respectively. Further, the P, QRS,

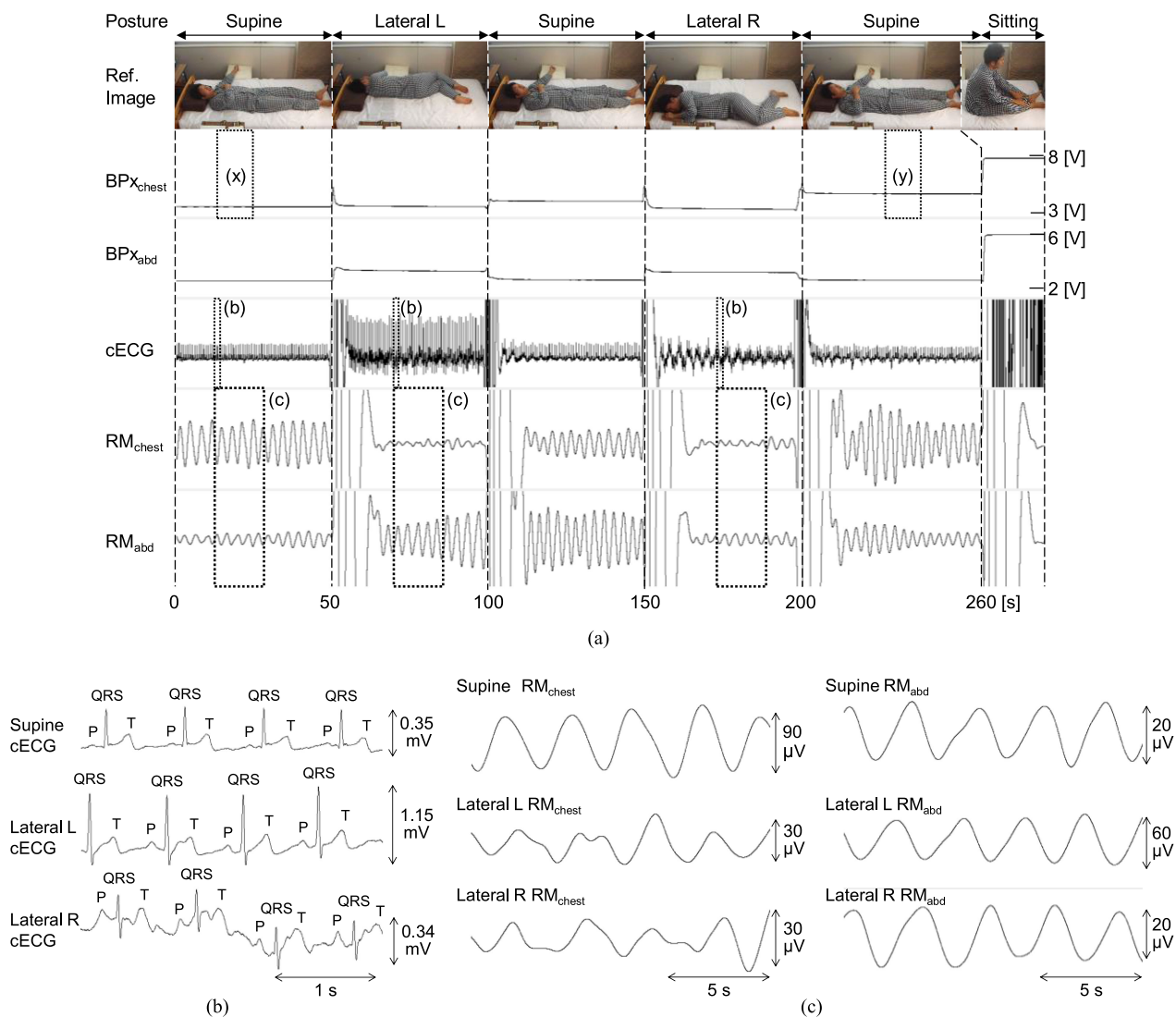


Fig. 5. Simultaneous measurements of subject #1 by the FUSE during resting with sequential postural changes. (a) Reference images of the subject lying on the bed and noncontact recordings of upper and lower BPxs, cECG, and RMs of the chest and abdomen. Body postures were measured over 30 s. (b) Enlarged cECG waveforms and (c) enlarged RM signals of the chest and abdomen corresponding to the dotted rectangular sections in the three body postures shown in (a).

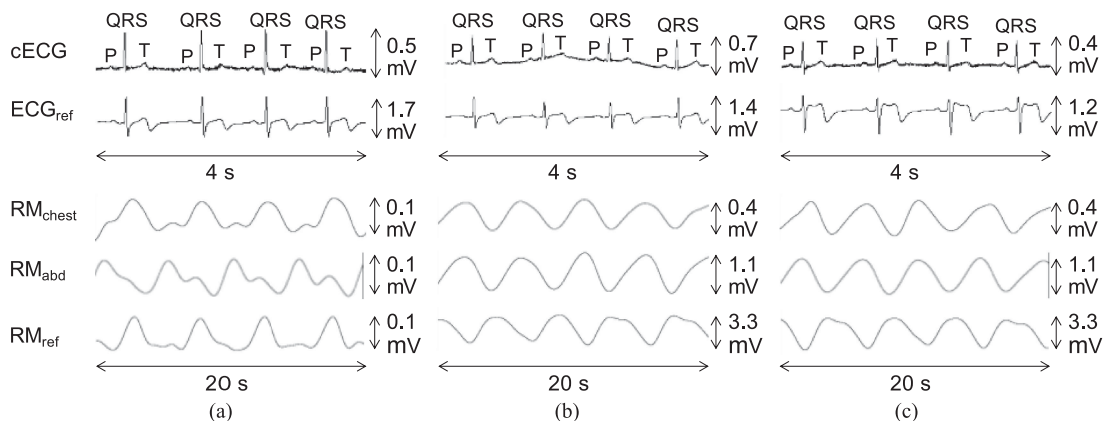


Fig. 6. Recording of cECG/ECG and RM signals from the proposed system and the reference systems during overnight experiment for subject #J. Sections were selected when the subject was in the (a) supine, (b) left lateral, and (c) right lateral postures.

TABLE II
 SENSITIVITY (P_{SNS}) [%], ACCURACY (P_{ACC}) [%], POSITIVE PREDICTIVE VALUE (P_{PPV}) [%] AND THE NUMBER OF REFERENCE DATA ($N_{TP} + N_{FN}$)
 FOR THE R WAVE AND T WAVE OF cECG AND CHEST AND ABDOMINAL RMs

Subject	cECG							RM						
	R wave			T wave			$N_{TP}+N_{FN}$	Chest			Abdominal			$N_{TP}+N_{FN}$
	P_{SNS}	P_{ACC}	P_{PPV}	P_{SNS}	P_{ACC}	P_{PPV}		P_{SNS}	P_{ACC}	P_{PPV}	P_{SNS}	P_{ACC}	P_{PPV}	
#J	76.0	76.0	100	74.9	70.4	92.3	16,969	93.6	86.6	92.0	92.2	82.4	88.5	4,385
#K	82.5	82.5	99.9	80.6	80.4	99.6	20,698	90.9	84.7	92.6	88.0	77.8	87.0	5,929
#L	92.0	92.0	99.9	92.6	83.3	88.3	18,603	92.5	82.4	88.3	96.1	91.6	95.1	5,424
#M	97.1	97.1	100	93.4	86.6	92.3	20,299	89.4	79.9	88.2	87.8	79.9	89.9	5,523
#N	83.5	83.4	99.9	83.4	78.2	92.4	23,005	82.4	73.9	87.8	82.4	75.5	90.0	4,469
#O	80.0	80.0	99.9	96.7	93.5	96.3	19,827	92.8	76.5	81.3	89.9	77.1	84.4	4,955
#P	91.8	91.8	100	94.4	94.4	99.9	19,993	93.1	89.1	95.4	94.5	92.6	97.7	5,395
MN	86.1	86.1	99.9	88.0	83.8	94.4	19,913	90.7	81.9	89.4	90.1	82.4	90.4	5,154
SD	± 7.6	± 7.6	± 0.1	± 8.3	± 8.5	± 4.3	$\pm 1,858$	± 3.9	± 5.5	± 4.5	± 4.6	± 7.0	± 4.6	± 573

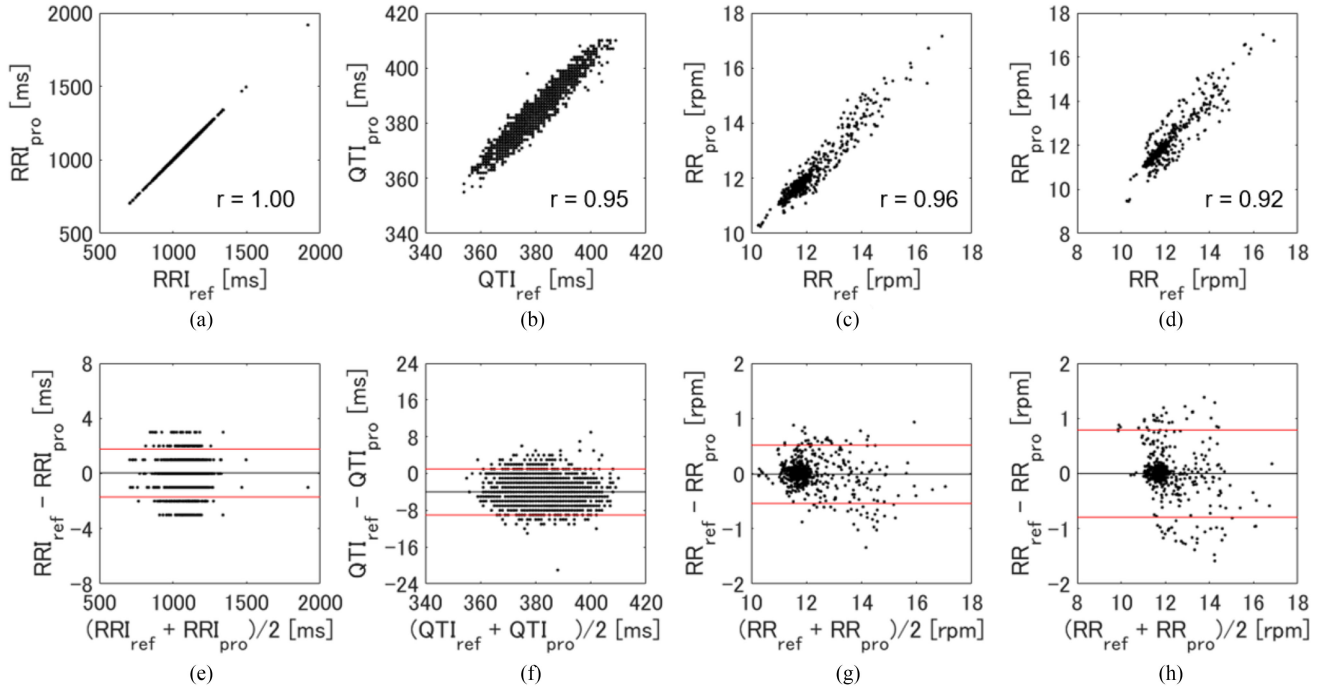


Fig. 7. Correlation plots of (a) RRI, (b) QTI, (c) RR on the chest and (d) RR on the abdomen between the reference and the proposed systems, and their Bland-Altman plots of (e) RRI, (f) QTI, (g) RR on the chest and (h) RR on the abdomen (Subject #J). All plots were calculated from a 4th 1-hour segment in the 6-hour recording. Subscript “ref” or “pro” on the each parameter indicates that the parameter is obtained from the “reference” or “proposed” system.

and T waves in cECG were automatically recognized in all LPs as with Fig. 5(b) by the same software written in V-C.

The P_{SNS} , P_{ACC} and P_{PPV} of each 6-h signal for each of the seven subjects are shown in Table II. The average P_{SNS} , P_{ACC} and P_{PPV} of cECG were 86.1%, 86.1% and 99.9% for the R wave and 88.0%, 83.8%, and 94.4%, respectively, for the T wave. The P_{SNS} and P_{ACC} for subject #J were below 80%, much lower than those for the other subjects, because subject #J twisted and turned frequently in the bed, resulting drastic changes in the waveform and amplitude of the cECG signal. On the other hand, the P_{SNS} (P_{ACC} , P_{PPV}) of RM_{chest} and RM_{abd} were 90.7% (81.9, 89.4%), and 90.1% (82.4, 90.4%), respectively. The P_{PPV} of RM_{chest} and RM_{abd} for subject #O were below 85%, much lower than those for the other subjects, because the numbers of falsely detected of RMs were higher the other subjects. Since the subject #O reported nocturnal awakenings, the higher numbers of false detection were considered due to small body movements

which were observed more frequently in his recordings than the other subjects.

Fig. 7 shows correlation plots of RRI, QTI, and RRs between the reference and proposed systems, and their Bland-Altman plots for subject #J. Correlation coefficients and double SDs of RRI, QTI and RRs for all subjects are shown in Table III. Both correlation coefficients of RRI and QTI were more than 0.90 in all subjects, showing high degree of accuracy. Further, the estimated errors for these intervals of the proposed system were within ± 3 and ± 11 ms, respectively. The correlation coefficients of RRs also showed a high degree of accuracy (> 0.90) with the exception of RM_{chest} of subject #L. The both estimated errors for RRs of our system were within ± 2 rpm.

Fig. 8(a) shows the distinctive waveforms measured during sleep, including during the periods before and after presumed apnea and/or hypopnea. In the absence of apnea, hypopnea, and body movement, the waveforms of the cECG and RM sig-

TABLE III
CORRELATION COEFFICIENT (R) AND DOUBLE SD FOR RRI, QTI, RR DURING 4TH 1-HOUR SEGMENT IN THE 6-HOUR RECORDING

Subject	RRI		QTI		RR on the chest		RR on the abdomen	
	r	$2SD$ [ms]	r	$2SD$ [ms]	r	$2SD$ [rpm]	r	$2SD$ [rpm]
#J	1.00	1.74	0.95	5.16	0.96	0.53	0.92	0.79
#K	1.00	2.11	0.93	9.38	0.94	1.02	0.96	0.81
#L	1.00	1.98	0.93	10.49	0.85	1.03	0.94	0.62
#M	1.00	1.46	0.94	7.00	0.96	1.08	0.94	0.90
#N	1.00	2.69	0.96	7.33	0.96	1.53	0.94	1.75
#O	1.00	2.45	0.96	6.25	0.90	1.22	0.93	1.01
#P	1.00	2.82	0.98	7.24	0.92	0.78	0.98	0.41

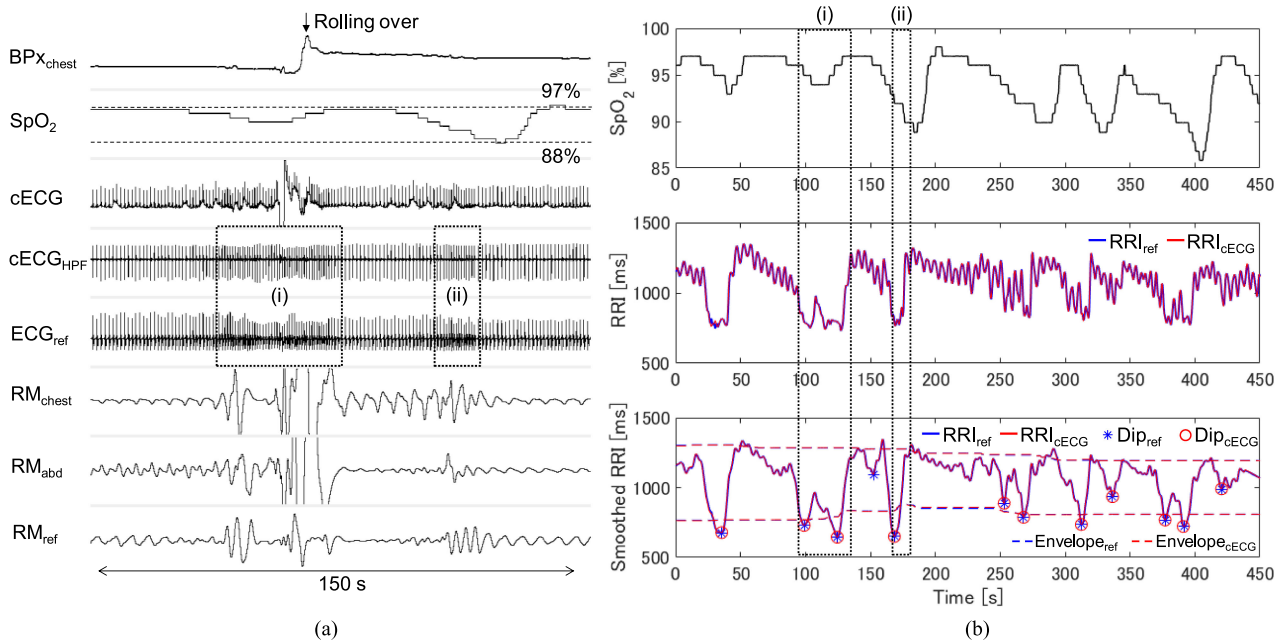


Fig. 8. Representative overnight measurements of subject #J showing apnea and/or hypopnea episodes. (a) Discriminative recordings of BPx at the chest, cECG, and RMs of the chest and abdomen measured by the FUSE and simultaneously recorded reference signals of SpO₂, ECG, and RM sensed by commercial measuring devices. cECG_{HPF} is the cECG waveform filtered through a high-pass filter (cutoff frequency = 10 Hz). The RRIs calculated from cECG_{HPF} and ECG_{ref} decreased significantly in the sections enclosed by the dotted rectangle. (b) Time series variation in SpO₂ (upper panel), RRI (middle panel), and smoothed RRI (lower panel). The RRI were calculated from cECG_{HPF} and ECG_{ref} at the times of the SpO₂ measurements and then interpolated with a spline function and resampled at 2 Hz. The smoothed RRI were computed from the RRI in the middle panel by a second-order polynomial fitting described in Hayano *et al.* [54]. Crosses and open circles in the smoothed RRI were detected by the dip detection algorithm in Hayano *et al.* [54]. The sections enclosed by the rectangular dotted line match those in (a).

nals were synchronized with the corresponding reference waveforms. However, around the occurrence of a body movement or breathing efforts associated with apnea or hypopnea involving a decrease in SpO₂, the waveform of the RM signal desynchronized from that of the RM_{ref} signal. In these cases, time was required to resume synchrony.

VI. DISCUSSION

A. Examination of Postural Distinction

The ability of our device to distinguish posture was evaluated in two experiments. Our system correctly classified the sitting postures of all subjects (Fig. 3 and Table I). The voltage was much higher in the sitting position than in the supine and lateral postures because the body was completely separated from the FUSE [see Fig. 5(a)]. On the other hand, the lateral posture

in subject #D was misclassified as supine, and the supine and lateral postures were confused in subjects #F and #G. Since the SDs of V_{BPx_abd} in the supine and lateral postures of subjects #D (0.27, 0.82 V) and #G (0.86, 1.24 V) were higher than in the other five subjects (0.08-0.15, 0.04-0.43 V), we consider repeatability of V_{BPx_abd} value was low in these subjects. In subject #F, the SDs of V_{BPx_abd} values in the supine and lateral postures (0.09, 0.15 V) were normal, but the MNs of V_{BPx_abd} values in these postures (3.02, 3.09 V) were close each other and indistinctive. In the lateral posture, the coupling area $A_{S(3)}$ or $A_{S(4)}$ between the upper body and one of the outer electrode of FUSE is probably smaller than in the supine position. Because a decrease in $A_{S(3)}$ or $A_{S(4)}$ also decreases the coupling capacitance $C_{BPx(3)}$ or $C_{BPx(4)}$ [see (4)], the output voltage $V_{out(3)}$ (i.e., V_{BPx_chest}) or $V_{out(4)}$ (i.e., V_{BPx_abd}) should increase slightly [see (5) and (6)]. However, magnitude relationship of V_{BPx_abd} values

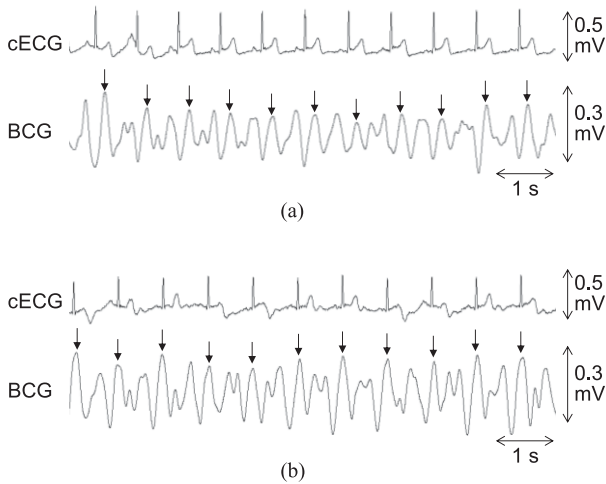


Fig. 9. Enlarged example of cECGs and possible BCGs of subject #I measured simultaneously by the FUSE during rest with sequential postural changes. The waveforms in panels (a) and (b) correspond to time sections x and y in Fig. 5, respectively. The arrows in the lower parts indicate the possible BCG peaks associated with the R waves of the cECGs in the upper parts.

between the supine and lateral positions was reversed in some segments of subjects #F and #G. This can be another reason for poor classification performance between the supine and lateral postures in subject #F and #G.

Similar phenomena are observed in Fig. 5(a). In Fig. 5(a), V_{BPx_chest} is larger in the second and third supine sequences than in the right- and left-lateral sequences; this behavior is not observed in the BPx_{abd} signals in this subject. Possible contributing factor is the coupling of the outer electrode (3) to the brachium and forearm in the lateral positions. As seen in the reference image of the right-lateral position in Fig. 5(a), the position of the subject's left elbow is closer to the shoulder line than in the supine positions. This might have increased the coupling area $A_{S(3)}$, resulting in a lower V_{BPx_chest} in the lateral positions.

Although our system correctly classified the sitting and lying positions, it should be further improved to distinguish among the various LPs. In the current model, the coupling capacitance in Fig. 2(b) assumes that $C_{S(3)} \ll C_G$. In contrast, the real electrode ratio is 27:1. Therefore, the detection P_{ACC} might be improved by narrowing the additional electrode. Using morphological information and cECG amplitude along with BPx signals might also be an effective to more accurately classify LPs.

B. Ability to Detect BCG

Fig. 9 shows the cECG and BCG signals that were measured simultaneously as described in Section IV-C. The wave pattern in Fig. 9(a) corresponds to section (x) of the initial supine position in Fig. 5(a). The BCG signal shows an apparent peak between the R and T waves of the cECG signal. Fig. 9(b) shows the wave pattern corresponding to section (y) of the third supine position (after four rolling movements). A similar peak in BCG following each cECG R wave can be confirmed in this wave pattern. A periodic peak with an amplitude of ~ 0.3 mV is also seen in the section corresponding to the second supine position

(after two rolling movements) in Fig. 5(a) (not shown). These results imply that the proposed system is able to measure BCG signals in the supine position after slight positional changes resulting from repeated rolling. However, such peaks were not observed in the section corresponding to the lateral position, likely because the subject's back separated from the FUSE in this posture, leaving only the shoulder coupled to the FUSE. In the lateral position, the upper outer electrode (3) shown in Fig. 1(b) cannot easily measure BCG, whereas the lower outer electrode (4) retains the contact pressure between the body and the FUSE. Therefore, in a future work, we will use the lower outer electrode (4) to measure BCG in the lateral lying position.

C. Evaluation of Overnight Measurements

As shown in Table II, the P_{SNS} and P_{ACC} of the R waves of cECG were identical for all subjects, and $MN \pm SD$ of the P_{PPV} was $99.9 \pm 0.1\%$. In other words, there was almost no false detection of R waves in the proposed system. On the other hand, the P_{PPV} of the T wave was 5.5 percentage points lower on average than the R wave. The primary reason for the false detection of the T waves was the wave-like baseline variation in the right-lateral position, which can be seen in Fig. 5(b). Both the R and T waves were less accurately measured in subjects #J and #K than in the other subjects. In subject #J, the P_{ACC} was lowest during the first 2 h of measurement, when the cECG signal gradually changed, and its amplitude fluctuated between 0.15 and 0.6 V. In subject #K, cECG detection became difficult when the amplitude diminished after a rolling-over movement. Since the SDs of P_{SNS} and P_{ACC} of the cECG were higher than those of the RMs, we can presume more individual or posture-dependent varieties of cECG waveform than those of RMs waveforms. As shown in Fig. 5(a), the cECG signal responded to postural changes in our proposed system. Therefore, cECG was difficult to detect in some sections using the present analysis algorithm because of drastic changes in its amplitude and waveform. To properly detect the cECG signal in difficult situations, the software must be improved to deal with changing cECG signals. This will be addressed in a future work.

In addition, one of the major factors that lowered detection performance of cECG was body movement. In previous work [56], we reported shortening of baseline restoration time of cECG from signal saturation after body movements by using driven seat ground (DSG) [57]. Therefore introduction of the DSG can be beneficial for the proposed system to mitigate influence of the body movements and to improve detection performance of cECG.

In the RM measurements of all subjects, the P_{ACC} was lower than the P_{SNS} (see Table II). The least P_{PPV} (81.3%) was found on the chest of subject #O, indicating a large number of false detections. One possible explanation for this discrepancy is the misclassification of baseline variation after a body movement as RM. Therefore, one of the next challenge to be addressed is to reduce influence of the body movements on RM detection by introducing some new methods such as singular spectrum analysis [58]. When comparing P_{ACC} between the chest and abdomen, the chest P_{ACC} was higher or lower than

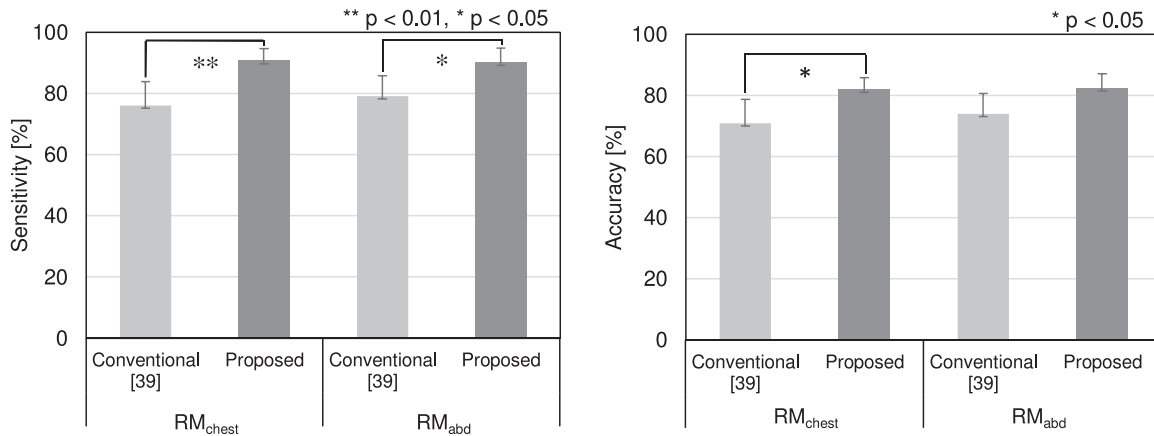


Fig. 10. Comparison of (a) sensitivity (P_{SNS}) and (b) accuracy (P_{ACC}) of the chest and abdominal RM signals between the conventional and proposed systems. The results of the conventional system are taken from [39]. The same subjects participated in both studies.

the abdominal P_{ACC} depending on the individual subject. This can reflect the different respiratory strategies of different individuals (i.e., chest respiration vs. abdominal respiration). Thus, it would be advantageous for the system to independently measure both chest and abdominal RMs.

Fig. 10 compares the average RM P_{SNS} and P_{ACC} of the proposed system and a conventional system [39]. All subjects participating in this test also participated in the overnight measurements performed in a previous study [39] and were assigned the same ID orders. The RM signals at the chest and abdomen were derived from the cECG signals in the conventional system, whereas they were derived from the BPx signals in the proposed system. The average P_{SNS} on the chest and abdomen were approximately 14 and 10 percentage points higher, respectively, in the proposed system than in the conventional system [Fig. 10(a)]. The greater P_{SNS} in the proposed system was significant ($p < 0.05$ for both RM_{chest} and RM_{abd}, paired t-test). The RM P_{ACC} of the proposed system were approximately 11 and 8 percentage points higher on the chest and abdomen, respectively, compared to those of the conventional system [Fig. 10(b)]. In the RM_{chest} measurements, both the P_{SNS} and P_{ACC} were higher for all subjects in the proposed system than in the conventional system. These results confirm the superiority of the proposed system over the conventional system in terms of RM measurement.

D. Detection of Apnea and/or Hypopnea

In a number of sections in the overnight test of subject #J, SpO₂ decreased by more than 3% [see Fig. 8(a)]. Since the result obtained from the apnea screening device showed 9.8 of AHI for this subject and detected multiple episodes of apnea/hypopnea in the segment shown in Fig. 8, the decreases in SpO₂ were assumed to be caused by apnea and/or hypopnea. Video recordings in this segment revealed many body movements (e.g., rolling-over movements and neck/hand movements) after the decrease in SpO₂. These body movements were measurable by the BPx signal in our proposed system.

As shown in Fig. 8(a), the baseline cECG fluctuated around the periods of decreased SpO₂; as a result, it was not clear whether the R wave was synchronized with the reference ECG

wave (i.e., ECG_{ref}). In contrast, in the high-pass-filtered cECG signal (i.e., cECG_{HPF}), the R waves were clearly visible, and RRI was easily calculated. Fig. 8(b) shows the time series of SpO₂, RRI, and smoothed RRI during the presumed apnea and/or hypopnea episodes. The dotted rectangular sections (i) and (ii) in Fig. 8(b) correspond to those in Fig. 8(a). The time series of RRI in the cECG (RRI_{cECG}) almost matches that in the ECG_{ref} [RRI_{ref}; see the middle panel of Fig. 8(b)]. In Fig. 8(b), recurring dips in both RRI_{cECG} and RRI_{ref} precede repetitive decreases in SpO₂. This precedence can stem from a long delay of SpO₂ calculation algorithm (at least 8 s in the used module OXY100C). Using the automatic detection algorithm proposed by Hayano *et al.* [54], a total of 12 dips in RRI were detected in the 450-s segment of smoothed RRI_{ref} shown in Fig. 8(b) (see the bottom panel). In contrast, 11 of the 12 dips were detected in the smoothed RRI_{cECG} at approximately the same times. Hayano *et al.* proposed an additional algorithm to compute the index of cyclic variation of heart rate (CVHRI) from the number of the dips and the time in bed [53]–[55]; they also proposed that CVHRI can be used in place of the apnea–hypopnea index to indicate the severity of sleep apnea.

Before the reduction in SpO₂, RM_{chest} and RM_{abd} were oppositely phased in Fig. 8(a). A preliminary test confirmed that when this subject ceased breathing, the amplitudes of RM_{chest} and RM_{abd} approached zero. In OSA, oppositely phased chest and abdominal movements are known to persist while the air-flow through the airway is blocked [59]. Therefore, we concluded that our proposed system captured the opposite phase of breathing effort caused by obstructive apnea and/or hypopnea in Fig. 8(a). After the reduction in SpO₂, the amplitudes of RM_{chest} and RM_{abd} became large and/or unstable, and the RM_{ref} behaved similarly. These behaviors may be explained by the body movements after effortful breathing. Because of the high sensitivity of the proposed system, the variation in amplitude was larger than RM_{ref}.

The above results suggest that apnea and/or hypopnea episodes can be accurately detected by simultaneously measuring cECG, two types of RM (at the chest and abdomen), postural changes, body movements (e.g., rolling movements),

and SpO₂. Since our proposed system simultaneously measures all the above parameters except SpO₂ without the attachment of transducers on the body in combination with a pulse oximeter, the proposed system might be applied in the detection of sleep apnea and/or hypopnea.

VII. CONCLUSION AND FUTURE WORKS

This study proposed a noncontact system that simultaneously measures multiple physiological and behavioral signals in recumbent humans. Measurements are performed by the FUSE, a flexible sensor system that can be placed under the bedclothes. The performance of the proposed system was tested in both short-term and overnight experiments. The system accurately classified the sitting postures and LPs and measured the cECG and RM signals in the supine and right-/left-lateral postures. cECG, two kinds of BPx, and RM signals were measured simultaneously. These signals are expected to be simultaneously measured with BCG in the supine posture. In the overnight experiment, the proposed system achieved improvements of 10–14 percentage points and 8–11 percentage points in average P_{SNS} and P_{ACC} of the RM signals, respectively, compared to the conventional system. Therefore, the proposed approach can be applied in to unobtrusively monitor physiological and behavioral signals in recumbent humans at night. In the cECG measurements, the waveform of the cECG responded to the posture of the sleeping subject. However, the P_{SNS} and P_{ACC} of the cECG measurements during sleep were below 90%. To improve upon these results, the analysis algorithm must be improved to accommodate cECG variation and tested on more participants in future studies.

REFERENCES

- [1] W. Lutz, W. Sanderson, and S. Scherbov, "The coming acceleration of global population ageing," *Nature*, vol. 451, no. 7179, pp. 716–719, Feb. 2008.
- [2] United Nations, "World population prospects: The 2012 revision," United Nations, New York, NY, USA, Tech. Rep. ESA/P/WP.228, 2013. [Online]. Available: https://esa.un.org/unpd/wpp/publications/Files/WPP2012_HIGHLIGHTS.pdf
- [3] Y. G. Lim *et al.*, "Monitoring physiological signals using noninvasive sensors installed in daily life equipment," *Biomed. Eng. Lett.*, vol. 1, no. 1, pp. 11–20, Feb. 2011.
- [4] C. Brüser, C. H. Antink, T. Wartzek, M. Walter, and S. Leonhardt, "Ambient and unobtrusive cardiorespiratory monitoring techniques," *IEEE Rev. Biomed. Eng.*, vol. 8, pp. 30–43, Mar. 2015.
- [5] P. A. Heidenreich *et al.*, "Forecasting the future of cardiovascular disease in the United States: A policy statement from the American Heart Association," *Circulation*, vol. 123, no. 8, pp. 933–944, Mar. 2011.
- [6] J. E. P. Waktare, "Atrial fibrillation," *Circulation*, vol. 106, no. 1, pp. 14–16, Jul. 2002.
- [7] E. Shahar *et al.*, "Sleep-disordered breathing and cardiovascular disease: Cross-sectional results of the sleep heart health study," *Amer. J. Respiratory Crit. Care Med.*, vol. 163, no. 1, pp. 19–25, Jan. 2001.
- [8] M. A. Konstam, "Home monitoring should be the central element in an effective program of heart failure disease management," *Circulation*, vol. 125, no. 6, pp. 820–827, Feb. 2012.
- [9] A. Darkins *et al.*, "Care coordination/home telehealth: The systematic implementation of health informatics, home telehealth, and disease management to support the care of veteran patients with chronic conditions," *Telemed. E-Health*, vol. 14, no. 10, pp. 1118–1126, Dec. 2008.
- [10] World Health Organization, "The top 10 causes of death," World Health Org., Geneva, Switzerland, [Online]. Available: <http://www.who.int/mediacentre/factsheets/fs310/en/>. Accessed on: Aug. 14, 2017.
- [11] D. D. Bacquer, G. D. Backer, M. Kornitzer, and H. Blackburn, "Prognostic value of ECG findings for total, cardiovascular disease, and coronary heart disease death in men and women," *Heart*, vol. 80, no. 6, pp. 570–577, Dec. 1998.
- [12] M. K. Bennett, M. Shao, and E. Z. Gorodeski, "Home monitoring of heart failure patients at risk for hospital readmission using a novel under-the-mattress piezoelectric sensor: A preliminary single centre experience," *J. Telemed. Telecare*, vol. 23, no. 1, pp. 60–67, Jan. 2017.
- [13] M. Etemadi, O. T. Inan, L. Giovangrandi, and G. T. A. Kovacs, "Rapid assessment of cardiac contractility on a home bathroom scale," *IEEE Trans. Inf. Technol. Biomed.*, vol. 15, no. 6, pp. 864–869, Nov. 2011.
- [14] D. D. He, E. S. Winokur, and C. G. Sodini, "An ear-worn vital signs monitor," *IEEE Trans. Biomed. Eng.*, vol. 62, no. 11, pp. 2547–2552, Nov. 2015.
- [15] R. P. Lewis, S. E. Rittgers, W. F. Forester, and H. Boudoulas, "A critical review of the systolic time intervals," *Circulation*, vol. 56, no. 2, pp. 146–158, Aug. 1977.
- [16] W. Chen and D. Gibson, "Mechanisms of prolongation of pre-ejection period in patients with left ventricular disease," *Brit. Heart J.*, vol. 42, no. 3, pp. 304–310, Sep. 1979.
- [17] A. Q. Javaid, H. Ashouri, S. Tridandapani, and O. T. Inan, "Elucidating the hemodynamic origin of ballistocardiographic forces: Toward improved monitoring of cardiovascular health at home," *IEEE J. Transl. Eng. Health Med.*, vol. 4, pp. 1–8, Mar. 2016.
- [18] J. H. Shin, K. M. Lee, and K. S. Park, "Non-constrained monitoring of systolic blood pressure on a weighing scale," *Physiol. Meas.*, vol. 30, no. 7, pp. 679–693, Jun. 2009.
- [19] H. C. Hanger, M. C. Ball, and L. A. Wood, "An analysis of falls in the hospital: Can we do without bedrails?" *J. Amer. Geriatrics Soc.*, vol. 47, no. 5, pp. 529–531, May 1999.
- [20] K. Rapp, C. Becker, I. D. Cameron, H. H. König, and G. Büchele, "Epidemiology of falls in residential aged care: Analysis of more than 70,000 demis from residents of Bavarian nursing homes," *J. Amer. Med. Directors Assoc.*, vol. 13, no. 2, pp. 187.e1–187.e6, Feb. 2012.
- [21] D. C. Ranasinghe, R. L. Shinmoto Torres, K. Hill, and R. Visvanathan, "Low cost and batteryless sensor-enabled radio frequency identification tag based approaches to identify patient bed entry and exit posture transitions," *Gait Posture*, vol. 39, no. 1, pp. 118–123, Jan. 2014.
- [22] J. V. Agostini, D. I. Baker, and S. T. Bogardus, "Prevention of falls in hospitalized and institutionalized older people," Agency Healthcare Res. Quality, Rockville, MD, USA, Evidence Rep./Technol. Assessment: Number 43, 2001.
- [23] E. Capezuti, G. Maislin, N. Strumpf, and L. Evans, "Side rail use and bed-related fall outcomes among nursing home residents," *J. Amer. Geriatrics Soc.*, vol. 50, no. 1, pp. 90–96, Jan. 2002.
- [24] World Health Organization, *WHO Global Report on Falls Prevention in Older Age: Epidemiology of Falls*. Geneva, Switzerland: WHO, 2007. [Online]. Available: http://www.who.int/xageing/publications/Falls_prevention/March.pdf
- [25] P. Kannus, H. Sievänen, M. Palvanen, T. Järvinen, and J. Parkkari, "Prevention of falls and consequent injuries in elderly people," *Lancet*, vol. 366, no. 9500, pp. 1885–1893, Dec. 2005.
- [26] N. V. Carroll, P. W. Slattum, and F. M. Cox, "The cost of falls among the community-dwelling elderly," *J. Managed Care Pharmacy*, vol. 11, no. 4, pp. 307–316, May 2005.
- [27] J. A. Stevens, P. S. Corso, E. A. Finkelstein, and T. R. Miller, "The costs of fatal and non-fatal falls among older adults," *Injury Prevention*, vol. 12, no. 5, pp. 290–295, Oct. 2006.
- [28] M. Reddy, S. S. Gill, and P. A. Rochon, "Preventing pressure ulcers: A systematic review," *J. Amer. Med. Assoc.*, vol. 296, no. 8, pp. 974–984, Aug. 2006.
- [29] A. Cano *et al.*, "Improving outcomes by implementing a pressure ulcer prevention program (PUPP): Going beyond the basics," *Healthcare*, vol. 3, no. 3, pp. 574–585, Jul. 2015.
- [30] J. McBride and A. Richardson, "A critical care network pressure ulcer prevention quality improvement project," *Nursing Crit. Care*, vol. 21, no. 6, pp. 343–350, Mar. 2015.
- [31] Y. Akita, K. Kawakatsu, C. Hattori, H. Hattori, K. Suzuki, and T. Nishimura, "Posture of patients with sleep apnea during sleep," *Acta Otolaryngologica Supplementum*, vol. 123, no. 543, pp. 41–45, Jul. 2003.

- [32] A. Oksenberg, I. Khamaysi, D. S. Silverberg, and A. Tarasiuk, "Association of body position with severity of apneic events in patients with severe nonpositional obstructive sleep apnea," *Chest*, vol. 118, no. 4, pp. 1018–1024, Oct. 2000.
- [33] Y. Kim, S. Yoo, C. Han, S. Kim, J. Shin, and J. Choi, "Evaluation of unconstrained monitoring technology used in the smart bed for u-health environment," *Telemed. E-Health*, vol. 17, no. 6, pp. 435–441, Jul. 2011.
- [34] A. Lopez, Jr. and P. C. Richardson, "Capacitive electrocardiographic and bioelectric electrodes," *IEEE Trans. Biomed. Eng.*, vol. BME-16, no. 1, p. 99, Jan. 1969.
- [35] Y. M. Chi, T. P. Jung, and G. Cauwenberghs, "Dry-contact and noncontact biopotential electrodes: Methodological review," *IEEE Rev. Biomed. Eng.*, vol. 3, pp. 106–119, Oct. 2010.
- [36] Y. G. Lim, K. K. Kim, and K. S. Park, "ECG recording on a bed during sleep without direct skin-contact," *IEEE Trans. Biomed. Eng.*, vol. 54, no. 4, pp. 718–725, Apr. 2007.
- [37] A. Ueno, Y. Akabane, T. Kato, H. Hoshino, S. Kataoka, and Y. Ishiyama, "Capacitive sensing of electrocardiographic potential through cloth from the dorsal surface of the body in a supine position: A preliminary study," *IEEE Trans. Biomed. Eng.*, vol. 54, no. 4, pp. 759–766, Apr. 2007.
- [38] A. Ueno and Y. Yama, "Unconstrained monitoring of ECG and respiratory variation in infants with underwear during sleep using a bed-sheet electrode unit," in *Proc. 30th Annu. Int. Conf. IEEE Eng. Med. Biol. Soc.*, Vancouver, BC, Canada, 2008, pp. 2329–2332.
- [39] M. Takano, S. Yamagishi, T. Ohmura, Y. Fukuoka, and A. Ueno, "Non-contact simultaneous measurements of electrocardiogram and respiratory movements using capacitive sheet electrodes," *Adv. Biomed. Eng.*, vol. 6, pp. 28–36, Mar. 2017.
- [40] H. J. Lee, S. H. Hwang, S. M. Lee, Y. G. Lim, and K. S. Park, "Estimation of body postures on bed using unconstrained ECG measurements," *IEEE J. Biomed. Health Informat.*, vol. 17, no. 6, pp. 985–993, Nov. 2013.
- [41] K. Ito, Y. Fukuoka, G. Cauwenberghs, and A. Ueno, "Noncontact sensing of electrocardiographic potential and body proximity by in-bed conductive fabrics," *Comput. Cardiol.*, vol. 40, pp. 523–526, Mar. 2013.
- [42] O. T. Inan *et al.*, "Ballistocardiography and seismocardiography: A review of recent advances," *IEEE J. Biomed. Health Informat.*, vol. 19, no. 4, pp. 1414–1427, Jul. 2015.
- [43] X. Zhu, W. Chen, T. Nemoto, K. Kitamura, and D. Wei, "Long-term monitoring of heart rate, respiration rhythm, and body movement during sleep based upon a network," *Telemed. E-Health*, vol. 16, no. 2, pp. 244–253, Mar. 2010.
- [44] S. Nukaya, T. Shino, Y. Kurihara, K. Watanabe, and H. Tanaka, "Noninvasive bed sensing of human biosignals via piezoceramic devices sandwiched between the floor and bed," *IEEE Sensors J.*, vol. 12, no. 3, pp. 431–438, Mar. 2012.
- [45] H. Brown, J. Terrence, P. Vasquez, D. W. Bates, and E. Zimlichman, "Continuous monitoring in an inpatient medical-surgical unit: A controlled clinical trial," *Amer. J. Med.*, vol. 127, no. 3, pp. 226–232, Mar. 2014.
- [46] A. Tal, Z. Shinar, D. Shaki, S. Codish, and A. Goldbart, "Validation of contact-free sleep monitoring device with comparison to polysomnography," *J. Clin. Sleep Med.* vol. 13, no. 3, pp. 517–522, Mar. 2017.
- [47] Y. Fukuyama, R. Suzuki, S. Takayama, and A. Ueno, "Multi-layered fabric electrode for movement artifact reduction in capacitive ECG measurement," in *Proc. 35th Annu. Int. Conf. IEEE Eng. Med. Biol. Soc.*, Osaka, Japan, 2013, pp. 555–558.
- [48] Y. Kato, S. Motohara, T. Omuta, A. Azran, and A. Ueno, "Artifact tolerance test for capacitive wearable chest-belt electrocardiograph-effect of electrode configuration," *IEEJ Trans. Electron. Inf. Syst.*, vol. 137, no. 4, pp. 607–615, Apr. 2017.
- [49] A. Ueno, Y. Shiogai, and Y. Ishiyama, "A primary study of indirect ECG monitor embedded in a bed for home health care," (in Japanese), *IEEJ Trans. Electron. Inf. Syst.*, vol. 127, no. 10, pp. 1792–1799, Oct. 2007.
- [50] S. Yamagishi, M. Takano, A. Ueno, and Y. Fukuoka, "A study on breath detection algorithm for capacitive in-bed cardiorespiratory monitor," (in Japanese), IEICE, Tokyo, Japan, Tech. Rep. MBE 2015-103, Mar. 2016, vol. 115.
- [51] T. Ohmura, K. Iimura, K. Mitsui, and N. Shibata, "Development of a QT measurement method by applying wavelet transform analysis and its correlation with QaT measurement," (in Japanese), *Jpn. J. Electrocardiol.*, vol. 26, no. 6, pp. 803–809, Nov. 2006.
- [52] H. C. Bazett, "An analysis of the time-relations of electrocardiograms," *History Electrocardiol.*, vol. 2, no. 2, pp. 177–194, Apr. 1997.
- [53] J. Hayano, "Cvhr shape measurement device," Patent WO2016143365, Nov. 15, 2016. [Online]. Available: <https://www.google.com/patents/WO2016143365A1?cl=en>
- [54] J. Hayano *et al.*, "Screening for obstructive sleep apnea by cyclic variation of heart rate," *Circulation: Arrhythmia Electrophysiol.*, vol. 4, pp. 64–72, Nov. 2011.
- [55] J. Hayano *et al.*, "Diagnosis of sleep apnea by the analysis of heart rate variation: A mini review," in *Proc. 33rd Annu. Int. Conf. IEEE Eng. Med. Biol. Soc.*, Boston, MA, USA, 2011, pp. 7731–7734.
- [56] M. Takano, H. Komiya, and A. Ueno, "Stability improvement and noise suppression in non-contact in-bed electrocardiogram measurement using laminated feedback electrode," in *Proc. IEEE Biomed. Circuits Syst. Conf.*, Torino, Italy, 2017, pp. 364–367.
- [57] K. K. Kim, Y. K. Lim, and K. S. Park, "Common mode noise cancelation for electrically non-contact ECG measurement system on a chair," in *Proc. 27th Annu. Int. Conf. IEEE Eng. Med. Biol. Soc.*, Shanghai, China, 2005, pp. 5881–5883.
- [58] F. Ghaderi, H. R. Mohseni, and S. Sanei, "Localizing heart sounds in respiratory signals using singular spectrum analysis," *IEEE Trans. Biomed. Eng.*, vol. 58, no. 12, pp. 3360–3367, Dec. 2011.
- [59] A. Murata, "Diagnosis and treatment of sleep apnea syndrome: Sleep apnea syndrome triggers life-threatening disorders during sleep," (in Japanese), *Nihon Ika Daigaku Igakkai Zasshi*, vol. 3, no. 2, pp. 96–101, May 2007.